



Characteristics and Sources of Speciated Atmospheric Mercury at a Coastal Site in the East China Sea Region

Lei Zhang¹, Long Wang¹, Shuxiao Wang^{1,2*}, Hongying Dou¹, Jianfeng Li¹, Shu Li¹, Jiming Hao^{1,2}

¹ School of Environment, and State Key Joint Laboratory of Environmental Simulation and Pollution Control, Tsinghua University, Beijing 100084, China

² State Environmental Protection Key Laboratory of Sources and Control of Air Pollution Complex, Beijing 100084, China

ABSTRACT

Atmospheric mercury is a global concern due to its ability of long-range transport. In order to understand the characteristics and sources of speciated mercury in the East China Sea region, a coastal monitoring site was established on Chongming Island in Shanghai, China. Total gaseous mercury (TGM), reactive gaseous mercury (RGM) and particulate-bound mercury (PHg) were monitored during 2009–2012. The overall average TGM, RGM and PHg concentrations were $2.65 \pm 1.73 \text{ ng m}^{-3}$, $8.0 \pm 8.8 \text{ pg m}^{-3}$ and $21.5 \pm 25.4 \text{ pg m}^{-3}$, respectively. TGM has a sharp increase at 5:00 in the morning and reaches peak at about 8:00, which is probably caused by the downward mixing of enhanced TGM aloft originated from regional sources. Wind roses suggest that urban Shanghai area has a considerable contribution to TGM in Chongming. Repartitioning of reactive mercury from particles to the air under the influence of air temperature could be one major source of RGM. Four heavy mercury pollution episodes were selected for source analysis. Mercury pollution in the summer event is mainly from the southwest direction with high $\Delta\text{TGM}/\Delta\text{CO}$ ratio and has the most influence on the North China Plain (NCP) region. The winter event is mainly under the influence of industrial pollution from the NCP region. The autumn event is contributed by both industrial pollution and biomass burning in North and Northeast China exhibiting a lower slope of $\Delta\text{PHg}/\Delta\text{TGM}$. Springtime Asian long-range transport (ALRT) is crucial to the mercury background of North America. However, in the spring event identified in this study the mercury outflow from low altitude through East China mostly ascended to high altitude during the transpacific airmass transport. This provides an important incentive for future studies to focus on the way of mercury outflow from East Asia.

Keywords: Speciated mercury; East China Sea region; Reactive mercury partitioning; HYSPLIT trajectories; Outflow.

INTRODUCTION

Mercury (Hg) is of crucial concern to public health and the global environment for its neurotoxicity, long-range transport, and bioaccumulation. Atmospheric Hg exists in three operationally defined forms: gaseous elemental mercury (GEM), reactive gaseous mercury (RGM) and particulate-bound mercury (PHg). GEM and RGM together are also known as total gaseous mercury (TGM). GEM originates from both natural and anthropogenic sources, and has a long residence time of 0.5–1 year (Driscoll *et al.*, 2013); RGM and PHg are from both primary sources and secondary formation and easy to be scavenged by wet and dry deposition due to high surface reactivity and water solubility (Schroeder and Munthe, 1998). The three Hg forms have mutual transformation. GEM can be converted to RGM in

the presence of atmospheric oxidants (e.g., Cl, Br, BrO, I, and OH) (Lin *et al.*, 2006; Subir *et al.*, 2011). RGM can be scrubbed by cloud or rain and then reduced to GEM by certain reductants (e.g., HO₂, SO₂, and SO₃²⁻) (van Loon *et al.*, 2000; Lin *et al.*, 2006). RGM can also be adsorbed onto particles in the atmosphere forming PHg. The distribution of reactive Hg between RGM and PHg depends on air temperature and aerosol species (Rutter and Schauer, 2007; Amos *et al.*, 2012; Cheng *et al.*, 2014a).

To characterize levels of different Hg forms and their distinct temporal and spatial trends, a number of monitoring sites have been established in China. These sites can be basically categorized into inland, coastal and oceanic sites. Inland sites can further be divided into urban, rural and remote sites. The Northern Hemisphere background Hg concentration has been declining from 1.5–1.7 ng m⁻³ (Lindberg *et al.*, 2007) to 1.3–1.5 ng m⁻³ (Slemr *et al.*, 2011). The average TGM concentrations at urban sites in some large cities in China, including Beijing, Nanjing, Guangzhou, Changchun, Guiyang and Chongqing are in the range of 6.7–18.4 ng m⁻³ (Fang *et al.*, 2004; Wang *et al.*, 2007; Yang

* Corresponding author.

E-mail address: shxwang@tsinghua.edu.cn

et al., 2009; Fu *et al.*, 2011; Zhu *et al.*, 2012). Urban sites in the southeastern coastal area of China, such as Shanghai, Ningbo and Xiamen, have relatively lower average TGM concentrations ($2.7\text{--}3.8\text{ ng m}^{-3}$) (Friedli *et al.*, 2011; Nguyen *et al.*, 2011; Xu *et al.*, 2015). Rural sites usually reflect regional backgrounds. Wang *et al.* (2007) reported an average background TGM for the Yangtze River Delta (YRD) region to be 5.4 ng m^{-3} , but only with a two-week campaign at a rural site in Jiaying. Our previous study (Zhang *et al.*, 2013) with one-year continuous observation at a rural site (Miyun) in the North China Plain (NCP) region showed the average GEM, RGM and PHg to be 3.2 ng m^{-3} , 8.9 pg m^{-3} and 98 pg m^{-3} , respectively. During a four-month campaign at a rural site in Hefei, a background site in the Central China region, Hu *et al.* (2014) found the average TGM and PHg to be 2.6 ng m^{-3} and 320 pg m^{-3} , respectively. Remote sites in mountainous area have the lowest TGM except for Mt. Gongga which is affected by Hg mining area in Southwest China. The average TGM concentrations at five remote sites (Mt. Gongga, Mt. Leigong, Mt. Changbai, Mt. Wanliguan and Shangri-La) were reported to be 4.0, 2.8, 1.6, 2.0 and 2.6 ng m^{-3} , respectively (Fu *et al.*, 2008, 2010a, 2012a, b; Zhang *et al.*, 2015).

Coastal and offshore marine sites are under the influence of both intensive inland anthropogenic sources and Hg evasion from marine water surface. Chand *et al.* (2008) found the average GEM, RGM and PHg in Okinawa in spring 2004 to be 2.0 ng m^{-3} , 3.0 pg m^{-3} and 4.5 pg m^{-3} , respectively. Nguyen *et al.* (2010) reported the average TGM in Jeju, Korea during 2006–2007 to be 3.9 ng m^{-3} . Two coastal sites in China are Chengshantou in the Yellow Sea region and Wanqingsha in the South China Sea region, where the average TGM concentrations were found to be 2.3 and 2.9 ng m^{-3} , respectively (Ci *et al.*, 2011a; Li *et al.*, 2011). Corresponding monitoring campaigns at two offshore marine sites in the Yellow Sea and South China Sea regions showed an average TGM level of 2.6 ng m^{-3} (Fu *et al.*, 2010b; Ci *et al.*, 2011b). However, there is little report on the East China Sea region which is one of the most important ports of Hg outflow from East Asia.

A coastal site on the estuary of Yangtze River to East China Sea was established in this study to evaluate the impacts of both anthropogenic sources in inland areas and clean air masses from marine boundary layer. Continuous monitoring of TGM and four campaigns of RGM and PHg were conducted during 2009–2012. We report the diurnal variations of different Hg forms and analyze their relationships with meteorological factors. Four typical heavy Hg pollution episodes in four seasons respectively were chosen for case study. Backward and forward trajectories for these four events were calculated to identify the source regions and track the Hg outflow through East China.

METHODOLOGY

Monitoring Site

The monitoring site ($31^{\circ}31'21''\text{N}$, $121^{\circ}54'31''\text{E}$, about 10 m asl) is at the top of the management office building of Dongtan Birds National Natural Reserve, Chongming

Island, Shanghai, China. As China's third largest island, Chongming is located in the East China Sea region with a typical subtropical monsoon climate. It is cold, dry and with northwestern wind in winter, and is hot, rainy with southern and southeastern winds in summer (see Fig. 1). There are no large anthropogenic sources on this island. The downtown Shanghai area was 50 km to the southwest of the site. There are no inhabitants within 5 kilometers but farmland and wetland. Speciated Hg concentrations here can reflect influence of Hg emission from the YRD region. As Chongming is at the very east of this region, the Hg outflow from mainland China can be embodied through long-term observation.

Monitoring Methods and QA/QC

Continuous 5-minute measurement of TGM was conducted with Tekran™ 2537B Hg vapor analyzer during three periods with all seasons covered: September 15 to December 17, 2009; July 14, 2010 to February 8, 2011; and November 28, 2011 to April 27, 2012. The instrument uses cold vapor atomic fluorescence spectroscopy (CVAFS) method with a detection limit of 0.1 ng m^{-3} (Landis *et al.*, 2002). During the sampling of ambient air, particles were removed by a 47-mm diameter Teflon filter at the inlet of the whole sampling system. The flow rate is constantly 1 L min^{-1} during all sampling periods.

Four campaigns for RGM and PHg were manually carried out using Tekran™ 2537B and the URG-2000 mercury sampling system: July 15 to August 13, 2010; October 10 to November 9, 2010; December 27, 2010 to January 29, 2011; and February 26 to March 25, 2012. The manual Hg monitoring system shown as Fig. S1 in the Supplementary Information (SI) contains the following key components: teflon coated elutriators with a cut point of $2.5\text{ }\mu\text{m}$ at a flowrate of 10 L min^{-1} ; two straight quartz tubes, of which one is a KCl-coated annular denuder for capturing RGM, and the other is a 21-mm diameter quartz membrane holder capturing $\text{PM}_{2.5}$ with PHg; a computerized pump used for sampling; and an insulated sampling box to control the temperature of the two tubes. During the campaigns, we obtained one valid sample for RGM and PHg every 2 hours, with one hour for sampling and another for analysis. In the sampling cycle, the flowrate of Tekran™ 2537B is 1 L min^{-1} and the flowrate of URG pump is set to be 9 L min^{-1} , making up a total flow of 10 L min^{-1} and capturing particles with an aerodynamic diameter of over $2.5\text{ }\mu\text{m}$. The tubes are maintained at a temperature of 50°C in the sampling box. In the analysis cycle, the Tekran™ 2537B analyzer and a Lindberg™ Blue M tube furnace are used. The KCl denuder and the quartz membrane holder are heated to 500°C and 800°C , respectively. Zero air goes through the heated tubes at a flowrate of 1 L min^{-1} into the analyzer. In a few 5-minute cycles, generally 4 for the denuder and 6 for the quartz fiber filter, Hg captured by the tubes is completely released to the analyzer, and the tubes are ready for the next sampling cycle. It should be noted that RGM measured by the denuder system could be underestimated. A significant loss (up to 80%) of mercury halides from KCl denuders could occur in the presence of ozone and absolute humidity

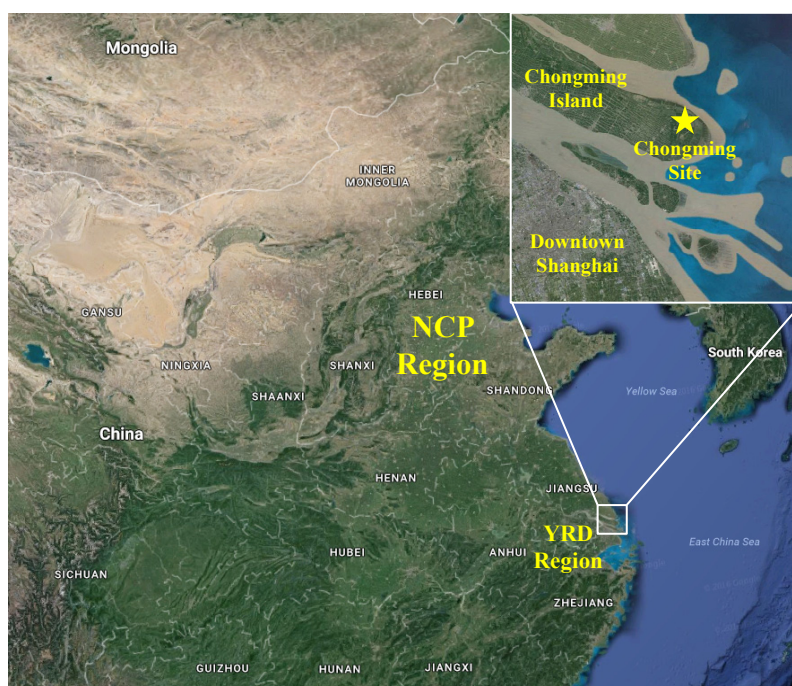


Fig. 1. The location of the Chongming monitoring site in Shanghai, China.

(Lyman *et al.*, 2010; Gustin *et al.*, 2013; McClure *et al.*, 2014; Huang and Gustin, 2015). However, this method is still the most accurate one so far and widely used for observation of speciated Hg in ambient air.

The analyzer is automatically calibrated every 25 hours by inner permeation with ZERO and SPAN processes for each cartridge. Peak areas for both cartridges during the calibration cycle are ensured to be 0 during the ZERO process and within an error of less than $\pm 10\%$ during the SPAN process. Manual calibration is performed once per six months with manual injection of mercury by a syringe from an external Hg source (Tekran™ 2505). The denuder is recoated every two weeks in case of passivation, following the procedure developed by Landis *et al.* (2002). The quartz membrane is changed once a month.

During the campaigns, CO, PM_{2.5} and black carbon (BC) were also monitored by Thermo Scientific Model 48CTL CO Analyzer, Thermo Scientific TEOM 1405D and Magee Scientific Aethalometer 42, respectively. Instrument details were discussed in our previous study (Wang *et al.*, 2008). The meteorological parameters including air temperature, wind speed and wind direction were measured by Vantage Pro2 weather station (Davis Instruments). All the data were hourly averaged in this study.

HYSPLIT Trajectory Analysis

In order to identify main sources of atmospheric Hg at Chongming site and track Hg outflow, three-dimensional air mass trajectories were calculated using the Hybrid Single-Particle Lagrangian Integrated Trajectory (HYSPLIT) model by the National Oceanic and Atmospheric Administration (NOAA) with gridded meteorological data from the Global Data Assimilation System (GDAS) at a horizontal resolution of $1^\circ \times 1^\circ$. Three starting heights were set to be 10 m, 100 m

and 200 m agl, respectively. We have identified four heavy TGM pollution episodes in summer (2010/7/29 3:00–2010/8/1 22:00), autumn (2010/10/29 18:00–2010/11/2 11:00), winter (2011/1/11 13:00–2011/1/12 8:00), and spring (2012/3/5 4:00–2012/3/7 4:00), respectively. Backward trajectories (120 h) and forward trajectories (240 h) were calculated every 6 hours for the four events.

RESULTS AND DISCUSSION

Characteristics of Speciated Hg Concentrations

Overall Statistics of Speciated Hg Concentrations

In the overall monitoring period, 8453 valid TGM hourly averages were obtained. Totally 1307 hours of RGM data and 1301 hours of PHg data were acquired during the four monitoring campaigns (one hour data every two hours due to the limitation of the manual method). The hourly averaged TGM is shown as Fig. S2 in the SI, and the hourly RGM and PHg are shown as Fig. S3 in the SI. TGM ranges from 0.70 to 18.37 ng m⁻³ with a mean of 2.65 ± 1.73 ng m⁻³ and a median of 2.08 ng m⁻³. The median value being smaller than the mean indicates that TGM is in a relatively low level near the background. The average TGM at Chongming site was 1.8–2 times the Northern Hemisphere background (Slemr *et al.*, 2011), close to those at other coastal sites in China (2.3 ng m⁻³ at Chengshantou site in the Yellow Sea region and 2.9 ng m⁻³ at Wanqingsha site in the South China Sea region) (Ci *et al.*, 2011a; Li *et al.*, 2011). RGM ranges from 0.1 to 69.2 pg m⁻³ with an average of 8.0 ± 8.8 pg m⁻³, close to reported rural or remote sites such as Mt. Gongga (6.2 pg m⁻³) (Fu *et al.*, 2008) and Miyun (8.9 pg m⁻³) (Zhang *et al.*, 2013). PHg ranges from 0.1 to 315.9 pg m⁻³ with an average of 21.5 ± 25.4 pg m⁻³, quite close to the level at the remote site Mt. Waliguan (19 pg m⁻³) (Fu *et al.*, 2012b).

Diurnal Variation of Speciated Hg Concentrations

TGM has a consistent diurnal pattern in four seasons as shown in Fig. 2(a). The TGM concentration is higher during the daytime. In all seasons, TGM reaches peak during 8:00–9:00 in the morning and decreases gradually to the minimum at about 20:00. During the nighttime, TGM is relatively stable especially in autumn. We can see the same peak at

about 8:00 in the morning in other coastal sites in China (Chenshantou and Wanqingsha) (Ci *et al.*, 2011a; Li *et al.*, 2011). At Chongming and Chenshantou, much sharper increase occurs at 5:00 in summer and autumn. This pattern was also found in three sites (one coastal, one urban and one rural) in the southeastern US (Nair *et al.*, 2012). There are two possible causes: a) the reemission of previously

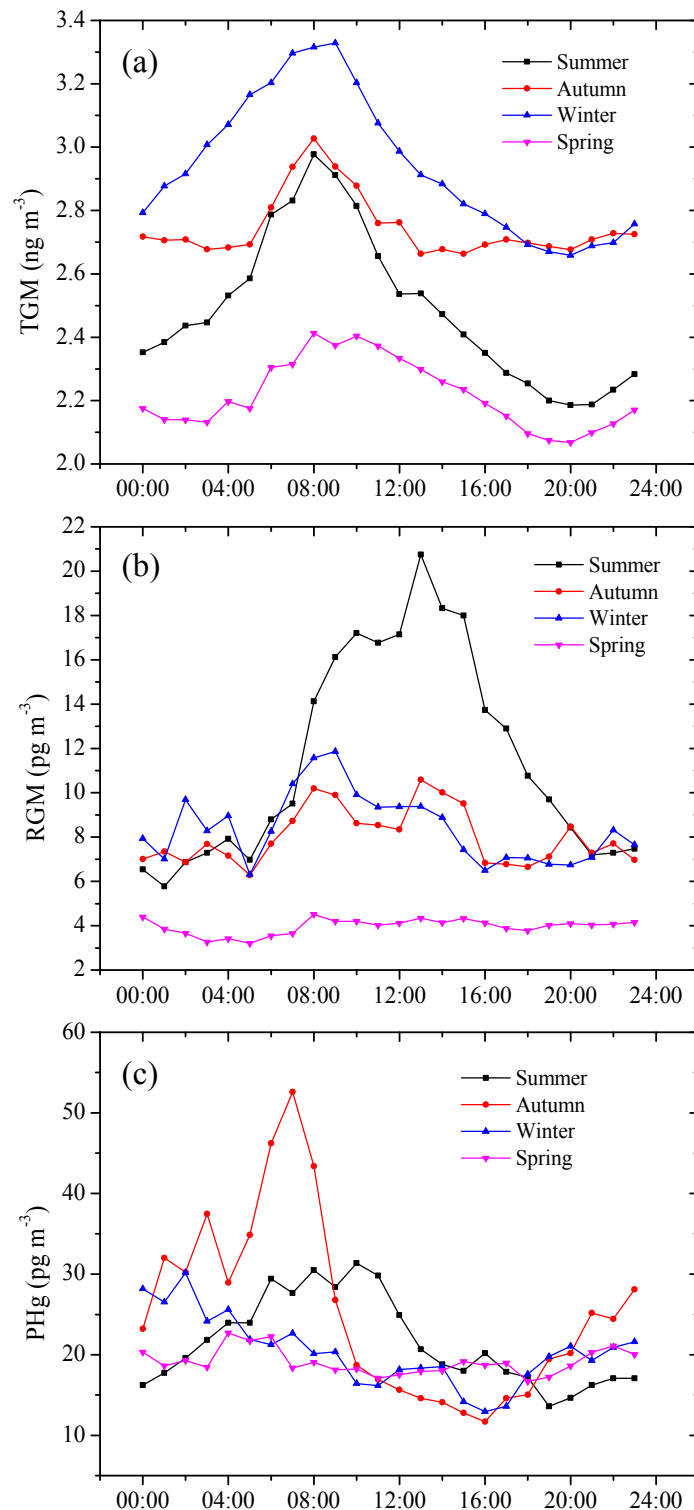


Fig. 2. Diurnal variation of (a) TGM, (b) RGM and (c) PHg in different seasons at local time.

deposited mercury to the atmosphere; and b) the downward mixing of enhanced TGM aloft originated from regional sources. The latter one could be the main cause because the diurnal patterns of TGM, RGM and PHg at Chongming are all affected. At a cleaner coastal site in Nova Scotia, Canada, GEM peak time occurs late (12:00–15:00) (Cheng *et al.*, 2014b). As the increase of wind speed in the early morning destroying the inversion layer, TGM decreases gradually during the daytime. In the night TGM exhibits a slight increase in spring, summer and winter. This trend is the same as the reported results in urban Shanghai area (Friedli *et al.*, 2011).

RGM in summer has a major peak at 14:00 in the afternoon (see Fig. 2(b)) while PHg has a decrease in the afternoon. This could be caused by the photochemical oxidation of GEM and the repartitioning of reactive Hg from particles to gaseous phase in summer (Ye *et al.*, 2016).

In spring and winter, the diurnal patterns of RGM are similar to TGM with a morning peak, but in autumn peaks can be observed both in the morning (8:00) and in the afternoon (14:00). As shown in Fig. 2(c), PHg has the similar pattern as TGM except for winter. The lowest PHg occurs at 16:00–18:00. In winter, PHg reaches peak in the midnight. The formation and increase of inversion layer from the evening time greatly influence all forms of mercury, and chemistry and transport also play important roles. In cleaner regions such as the coastal site in Nova Scotia, Canada, both RGM and PHg have peak time in the afternoon (12:00–15:00) (Cheng *et al.*, 2014b).

Relationships with Meteorological Factors

Influence of Wind Speed and Direction on TGM

Wind direction is the most direct evidence for spatial sources of atmospheric Hg. Fig. 3 shows the wind direction

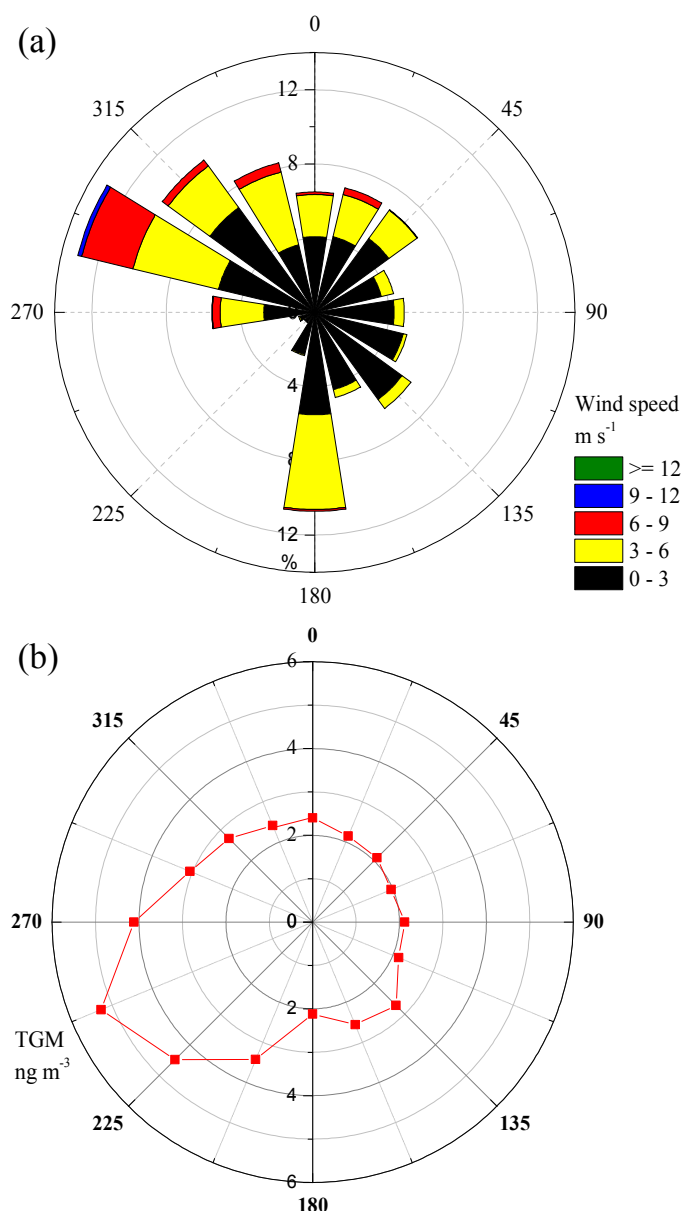


Fig. 3. Roses of (a) wind direction frequency and (b) average TGM concentration during the sampling periods.

frequencies with wind speeds and the average TGM concentrations in different directions. The most predominant wind directions are northwest and south, pointing to the YRD region and furthermore the NCP region. Average TGM is over 3 ng m^{-3} when air mass is from the southwest direction, much larger than from other directions. One reason for this is that the frequencies of wind from these directions are relatively small (0.7%, 0.9% and 5.6% for SW, NSW and W) and high values caused by Hg pollution events greatly increase the mean. A more important reason is that air mass from these directions carries Hg from the urban area of Shanghai which is much closer to the Chongming site and with higher Hg emission intensity. When wind is coming from the sea (northeast, east and southeast), average TGM is about $2\text{--}2.5 \text{ ng m}^{-3}$, indicating the background TGM level of East Asia. The TGM difference between northwest and southeast is about $0\text{--}1 \text{ ng m}^{-3}$, embodying the Hg outflow going from the inland area of China through the southeastern and eastern parts of China to the East China Sea region.

Influence of Air Temperature on Reactive Hg Partitioning

Air temperature is another important meteorological factor for speciated Hg, especially the partitioning of reactive Hg

between RGM and PHg, which was defined in the study of Rutter and Schauer (2007) as Eq. (1):

$$K = \frac{\text{PHg} / \text{PM}_{2.5}}{\text{RGM}} \quad (1)$$

where RGM, PHg and $\text{PM}_{2.5}$ are the concentrations of these pollutants, and K is the partitioning coefficient. K is highly related to air temperature followed by the van't Hoff equation:

$$\log_{10}(K^{-1}) = a - \frac{b}{T} \quad (2)$$

where a and b are constant coefficients and T is air temperature. The correlation between K and T in this study is shown as Fig. 4. The overall correlation regression fit is $\log_{10}(K^{-1}) = (12 \pm 1) - (3092 \pm 196)/T$ ($R^2 = 0.33$). From Fig. 4 we can see that the slope of the trend line for summer ($b = 12800 \pm 3000$, $R^2 = 0.16$) is much higher than for autumn and spring, which is mainly due to the high air temperature in summer. Table 1 shows the comparison of regression coefficients in different studies. The urban

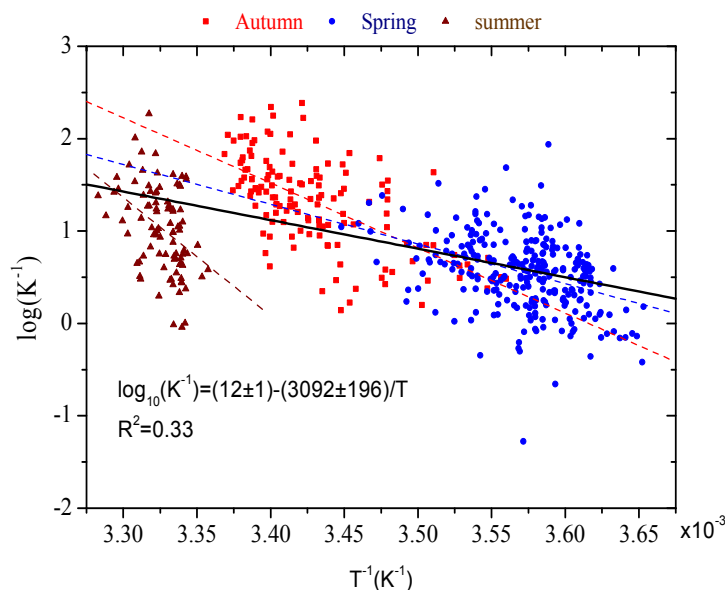


Fig. 4. Correlation between gas-particle mercury partitioning coefficient and air temperature.

Table 1. Regression coefficients for $\log_{10}(K^{-1}) = a - b/T$.

| Monitoring site | a | b | R^2 | Reference |
|--------------------------|------------|-----------------|-------|---------------------------|
| Chongming | 12 ± 1 | 3092 ± 196 | 0.33 | This study |
| Kejimkujik National Park | 15 ± 2 | 4286 ± 461 | 0.59 | Cheng et al. (2014a) |
| Underhill | 12 ± 1 | 3259 ± 225 | 0.54 | Cheng et al. (2014a) |
| Experimental Lakes | 9 ± 4 | 2400 ± 1100 | 0.57 | Amos et al. (2012) |
| Milwaukee | 7 ± 2 | 1900 ± 400 | 0.43 | Amos et al. (2012) |
| Pensacola | 6 ± 2 | 1600 ± 600 | 0.16 | Amos et al. (2012) |
| Reno | 13 ± 2 | 3300 ± 600 | 0.54 | Amos et al. (2012) |
| Thompson Farm | 8 ± 6 | 2000 ± 1600 | 0.33 | Amos et al. (2012) |
| Milwaukee and Riverside | 15 ± 2 | 4250 ± 480 | 0.77 | Rutter and Schauer (2007) |
| Milwaukee | 7 ± 1 | 1710 ± 380 | 0.49 | Rutter and Schauer (2007) |

Riverside site in the study of Rutter and Schauer (2007), the Reno site in the study of Amos *et al.* (2012) and the two coastal/rural sites in the study of Cheng *et al.* (2014a) reveal high b values. All of these sites have higher temperature ranges. Similar as the summer case in this study, these evidences indicate that high air temperature could affect the adsorption-desorption balance on the surface of particles and reinforce the influence of temperature on the partitioning process. Chongming shows a relatively high slope, driving the reactive Hg balance more towards the desorption direction. According to the diurnal pattern in summer, RGM exhibits a significant increase after 12:00 while PHg decreases, indicating that repartitioning of reactive Hg from particles to gaseous phase could be one of the major sources of RGM in the YRD region.

Sources of Atmospheric Hg in Heavy Pollution Episodes *Backward Trajectories in Heavy Pollution Episodes*

Fig. 5 shows the backward trajectories for four heavy Hg pollution episodes in four seasons respectively. Hg pollution in the summer event is mainly from the southwest direction to the monitoring site at a low altitude level while pollution from the autumn, winter and spring events is from the north. The urban Shanghai area is to the southwest of the Chongming site, being the closest source to it. The short lifetime of RGM and the strong photochemical oxidation condition in urban area both contribute to high impact of the urban Shanghai area on RGM elevation in summer. The autumn and winter events originate from Siberia and go through Mongolia, Inner Mongolia and the NCP region. The trajectories have low altitude levels in the NCP region, which enhances the influence of heavy Hg pollution from the NCP region in heating seasons (the whole winter and partially autumn). The heights of the trajectories in Siberia, Mongolia and Inner Mongolia are lower in the autumn event than in the winter one, indicating more impacts from these regions in autumn. Biomass burning and industrial pollution in North and Northeast China lead to high PHg in autumn. The airmass in the spring event originates from high altitude in Siberia, takes a detour through Northeast China, and thus to some extent avoids the heaviest pollution in the Beijing-Tianjin-Hebei region, resulting in the mildest Hg pollution in spring.

Correlations between Multi-Pollutants in Heavy Pollution Episodes

Correlations between different mercury forms, CO and BC were calculated for the four heavy pollution episodes, as shown in Table 2. The autumn event has the highest mean TGM, while the winter event has the highest averages of RGM and PHg. No significant correlations were found between RGM and TGM in all the events except for the spring one. In the meantime, the spring event has the lowest RGM average. Strong correlation between TGM and PHg ($R^2 = 0.63$) was found in the autumn event with a lower $\Delta\text{PHg}/\Delta\text{TGM}$ slope (14 pg ng^{-1}) than in the summer and spring events ($\sim 20 \text{ pg ng}^{-1}$). It reflects the contribution of biomass burning in North and Northeast China in the autumn event (Fig. 5(b)). Plumes from biomass burning have higher temperature than from industrial pollution. The balance

between RGM and PHg could be driven more towards the desorption direction, leading to lower $\Delta\text{PHg}/\Delta\text{TGM}$ in plumes from biomass burning compared to industrial plumes. Further research is needed to verify this.

Industrial combustion processes usually have higher $\Delta\text{TGM}/\Delta\text{CO}$ (or $\Delta\text{GEM}/\Delta\text{CO}$) than biomass burning because smoldering biomass burning produce more CO. For typical Asian long-range transport (ALRT), mixed airmass under the influence of Siberian biomass burning and Asian industrial pollution departs from East Asia exports such as Okinawa. The slope of $\Delta\text{GEM}/\Delta\text{CO}$ at Okinawa site in the spring plume events in 2004 ranges from $3.6\text{--}7.4 \text{ ng m}^{-3} \text{ ppmv}^{-1}$ with an average value of $5.6 \text{ ng m}^{-3} \text{ ppmv}^{-1}$ (Jaffe *et al.*, 2005). After transpacific transport, it arrives in North America. The slope of $\Delta\text{GEM}/\Delta\text{CO}$ at a typical receptor site, Mt. Bachelor Observatory (MBO) in the western US, was reported to be $5.0 \text{ ng m}^{-3} \text{ ppmv}^{-1}$ in 2004 (Jaffe *et al.*, 2005). The summer event in Chongming has a high slope of $\Delta\text{TGM}/\Delta\text{CO}$ ($7.4 \text{ ng m}^{-3} \text{ ppmv}^{-1}$) with a strong correlation ($R^2 = 0.68$), while $\Delta\text{TGM}/\Delta\text{CO}$ for the autumn event was $5.0 \text{ ng m}^{-3} \text{ ppmv}^{-1}$, closer to those reported in Okinawa and MBO. This indicates that the summer event is under more influence of industrial pollution from the urban Shanghai area and further the southern YRD region while the autumn event is under the impact of both biomass burning and industrial pollution from North and Northeast China. Considerable correlation between BC and PHg ($R^2 = 0.41$) in the summer event could also be an indicator of the industrial contribution.

Outflow of Atmospheric Hg in Heavy Pollution Episodes

Fig. 6 shows the 10-day forward trajectories of the four heavy pollution episodes. The summer event has the most transpacific trajectories, most of which rise to high altitude level and a small part of which arrive in North America (Alaska and western Canada). However, most low-elevation parts of the trajectories have more influence on the NCP region. The autumn event has the most influence on the southeastern and southern part of China, and the trajectories continue to Southeast Asia, some of which even reach India but at a higher altitude. The winter event mostly affects Southeast Asia. Most trajectories for the spring event travel through the southeastern and southern parts of China and end up in Southeast Asia, while some travel across the Pacific Ocean and rise to high altitude in North America. To sum up, atmospheric Hg pollution in spring and summer has the most impact on the inland area in China. Springtime ALRT is crucial to the Hg background of North America (Jaffe *et al.*, 2005). However, in the spring event identified in this study the Hg outflow from low altitude through East China mostly ascends to high altitude during the transpacific airmass transport. Therefore, it is likely that some Asian plumes from biomass burning and industrial pollution have ascended to high altitude before they reach the East China export while the ALRT events starting from the East China Sea region at a low altitude might have less impact on the western North America. More studies are needed on the ALRT contribution of Hg to North America. In the meantime, the Hg outflow from East China to Southeast Asia in autumn and winter deserves more attention.

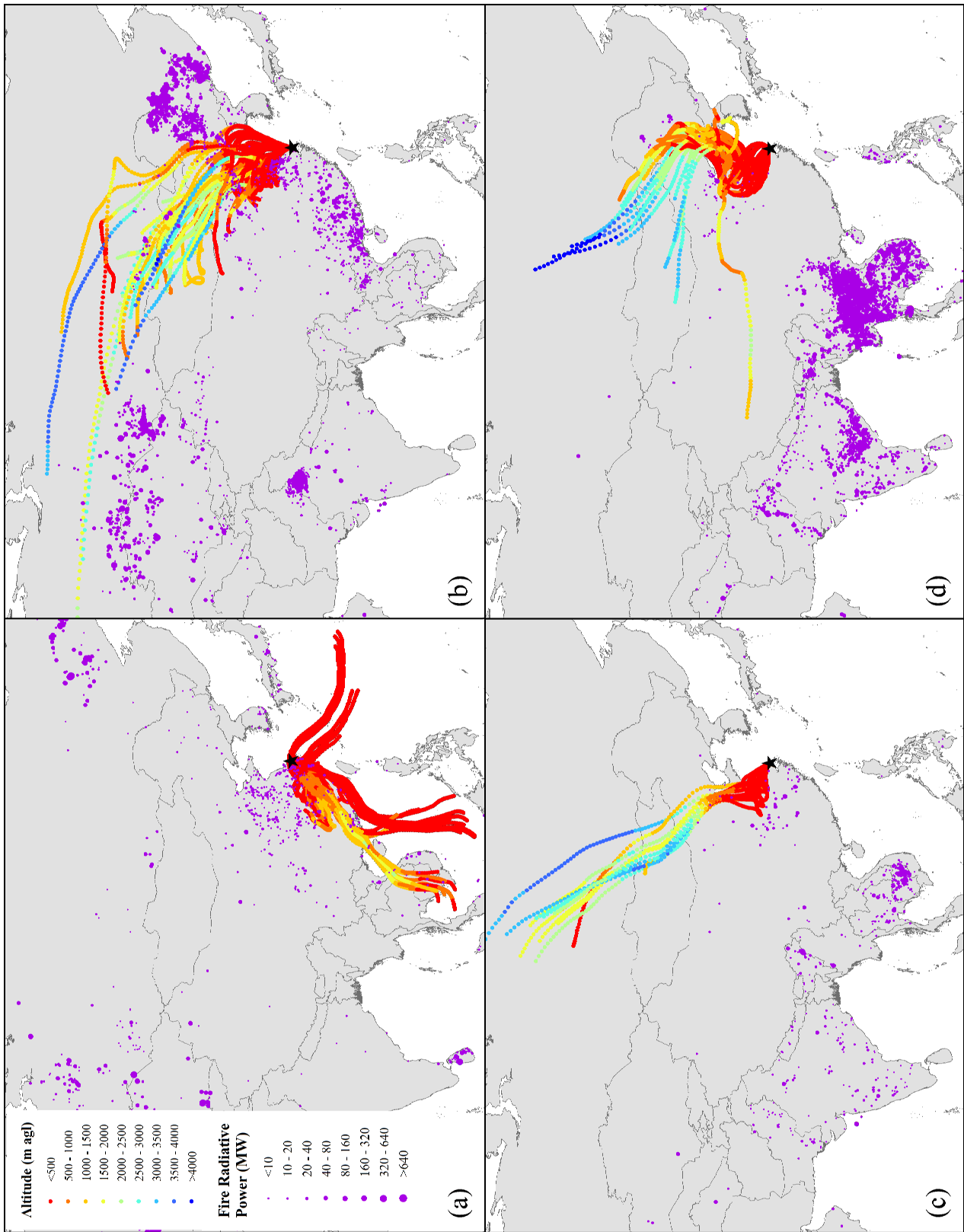
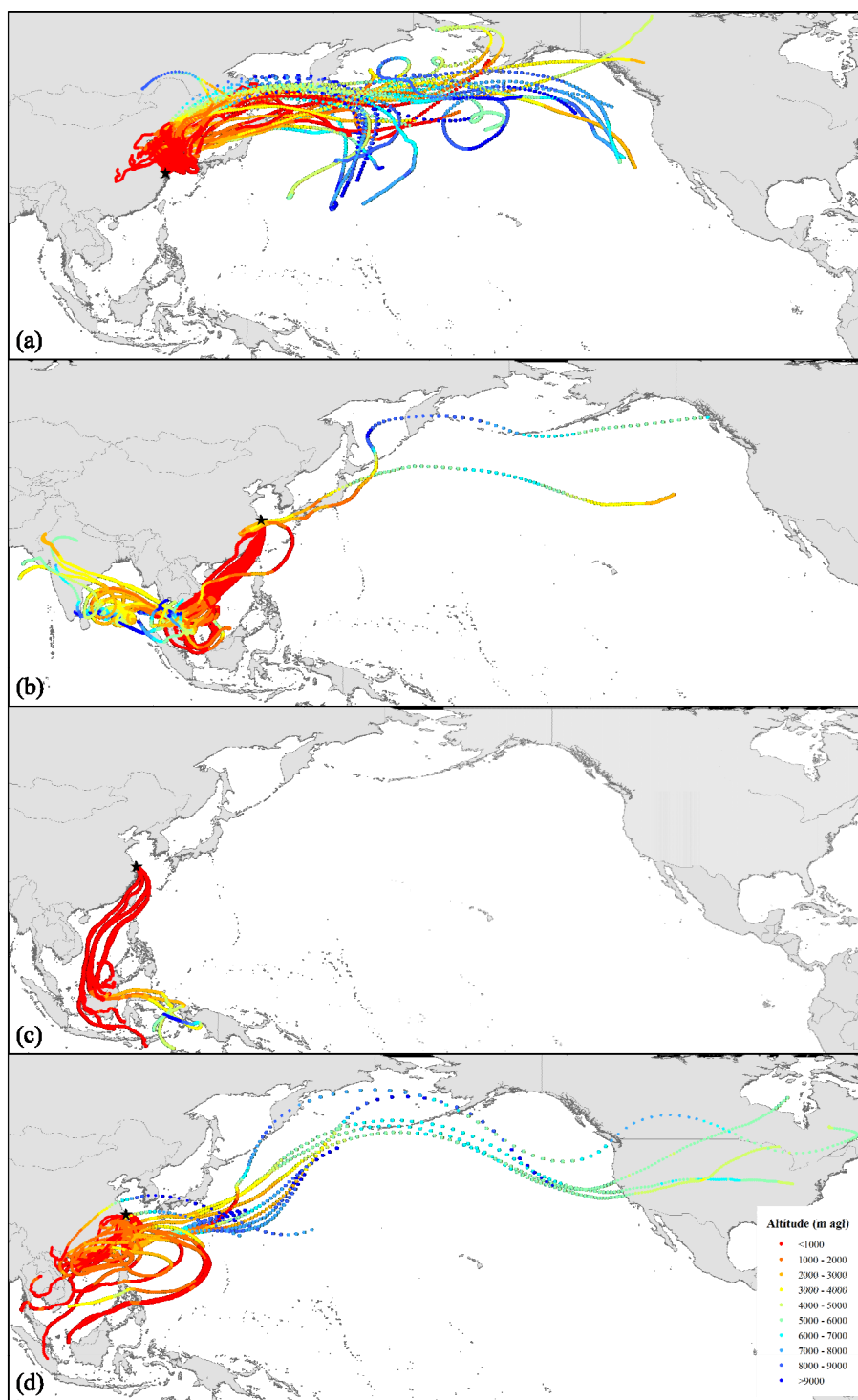


Fig. 5. Backward trajectories for the four heavy pollution episodes in (a) summer, (b) autumn, (c) winter, and (d) spring.

Table 2. Mean speciated mercury concentrations and multi-pollutant correlations for the four heavy pollution episodes.

| No. | Season | TGM (ng m^{-3}) | RGM (pg m^{-3}) | PHg (pg m^{-3}) | $\Delta\text{RGM}/\Delta\text{TGM}$ (pg ng^{-1}) | R^2 | $\Delta\text{PHg}/\Delta\text{TGM}$ (pg ng^{-1}) | R^2 | $\Delta\text{TGM}/\Delta\text{CO}$ ($\text{ng m}^{-3} \text{ppmv}^{-1}$) | R^2 | $\Delta\text{PHg}/\Delta\text{BC}$ ($\text{pg } \mu\text{g}^{-1}$) | R^2 |
|-----|--------|-------------------------------|-------------------------------|-------------------------------|--|-------|--|-------|---|-------|---|-------|
| 1 | Summer | 4.81 | 24.14 | 55.58 | – | 0.00 | 20.48 | 0.43 | 7.39 | 0.68 | 13.13 | 0.41 |
| 2 | Autumn | 7.17 | 13.44 | 50.49 | – | 0.12 | 14.15 | 0.63 | 5.04 | 0.40 | – | 0.25 |
| 3 | Winter | 4.50 | 37.75 | 60.83 | – | 0.26 | – | 0.07 | N.D. | N.D. | – | 0.01 |
| 4 | Spring | 5.06 | 6.56 | 49.16 | 1.82 | 0.37 | 20.56 | 0.37 | N.D. | N.D. | N.D. | N.D. |

Notes: N.D. refers to no data available; the slopes of not significant correlations ($R^2 < 0.3$) are not presented.

**Fig. 6.** Forward trajectories for the four heavy pollution episodes in (a) summer, (b) autumn, (c) winter, and (d) spring.

CONCLUSIONS

Monitoring campaigns for speciated mercury were conducted at a coastal site in the East China Sea region in this study during 2009–2012. RGM and PHg were observed based on a manual monitoring system. The overall average TGM concentration was found to be $2.65 \pm 1.73 \text{ ng m}^{-3}$, about 1.8–2 times of the background concentration of Northern Hemisphere. RGM and PHg are 8.0 ± 8.8 and $21.5 \pm 25.4 \text{ pg m}^{-3}$ respectively, close to reported rural or remote sites. Wind roses indicate considerable contribution of TGM from the urban Shanghai area. The oxidation of GEM and the repartitioning of reactive Hg from particles to gaseous phase could be two major sources of RGM in the YRD region. TGM has a sharp increase at 5:00, reaches peak during 8:00–9:00 in the morning and decreases gradually until the evening, which is probably caused by the downward mixing of enhanced TGM aloft after sunrise. The diurnal patterns of all Hg forms imply the influence of temperature inversion layer.

Trajectory analysis and multi-pollutant correlation analysis were performed for four typical Hg pollution events. The trajectories in the summer event are mainly from the southwest direction to the monitoring site with high $\Delta\text{TGM}/\Delta\text{CO}$. They travel north affecting the NCP region, and then transport across the Pacific Ocean ascending to high altitude. Industrial pollution in the NCP region contributes to the Hg pollution in heating seasons. Plumes from biomass burning with a lower slope of $\Delta\text{PHg}/\Delta\text{TGM}$ have considerable impact on the autumn event. The spring event bears the mildest Hg pollution among all four events but has the most influence on inland China, especially the southeastern and southern parts of China. Forward trajectories in the spring event suggest that the Hg outflow from low altitude through East China mostly ascends to high altitude during the transpacific air mass transport.

ACKNOWLEDGMENT

This work was sponsored by Major State Basic Research Development Program of China (973 Program) (No. 2013CB430003) and Natural Science Foundation of China (No. 21521064). We would like to thank Dr. Leiming Zhang (Environment Canada) for his valuable suggestions on this paper.

SUPPLEMENTARY MATERIAL

Supplementary data associated with this article can be found in the online version at <http://www.aaqr.org>.

REFERENCES

- Amos, H.M., Jacob, D.J., Holmes, C.D., Fisher, J.A., Wang, Q., Yantosca, R.M., Corbitt, E.S., Galarneau, E., Rutter, A.P., Gustin, M.S., Steffen, A., Schauer, J.J., Graydon, J.A., St Louis, V.L., Talbot, R.W., Edgerton, E.S., Zhang, Y. and Sunderland, E.M. (2012). Gas-particle partitioning of atmospheric Hg(II) and its effect on global mercury deposition. *Atmos. Chem. Phys.* 12: 591–603.
- Chand, D., Jaffe, D., Prestbo, E., Swartzendruber, P.C., Hafner, W., Weiss-Penzias, P., Kato, S., Takami, A., Hatakeyama, S. and Kajii, Y. (2008). Reactive and particulate mercury in the Asian marine boundary layer. *Atmos. Environ.* 42: 7988–7996.
- Cheng, I., Zhang, L.M. and Blanchard, P. (2014a). Regression modeling of gas-particle partitioning of atmospheric oxidized mercury from temperature data. *J. Geophys. Res.* 119: 11864–11876.
- Cheng, I., Zhang, L.M., Mao, H.T., Blanchard, P., Tordon, R. and Dalziel, J. (2014b). Seasonal and diurnal patterns of speciated atmospheric mercury at a coastal-rural and a coastal-urban site. *Atmos. Environ.* 82: 193–205.
- Ci, Z.J., Zhang, X.S., Wang, Z.W. and Niu, Z.C. (2011a). Atmospheric gaseous elemental mercury (GEM) over a coastal/rural site downwind of East China: Temporal variation and long-range transport. *Atmos. Environ.* 45: 2480–2487.
- Ci, Z.J., Zhang, X.S., Wang, Z.W., Niu, Z.C., Diao, X.Y. and Wang, S.W. (2011b). Distribution and air-sea exchange of mercury (Hg) in the Yellow Sea. *Atmos. Chem. Phys.* 11: 2881–2892.
- Driscoll, C.T., Mason, R.P., Chan, H.M., Jacob, D.J. and Pirrone, N. (2013). Mercury as a global pollutant: Sources, pathways, and effects. *Environ. Sci. Technol.* 47: 4967–4983.
- Fang, F.M., Wang, Q.C. and Li, J.F. (2004). Urban environmental mercury in Changchun, a metropolitan city in Northeastern China: Source, cycle, and fate. *Sci. Total Environ.* 330: 159–170.
- Friedli, H.R., Arellano, A.F., Geng, F., Cai, C. and Pan, L. (2011). Measurements of atmospheric mercury in Shanghai during September 2009. *Atmos. Chem. Phys.* 11: 3781–3788.
- Fu, X.W., Feng, X.B., Zhu, W.Z., Wang, S.F. and Lu, J.L. (2008). Total gaseous mercury concentrations in ambient air in the eastern slope of Mt. Gongga, South-Eastern fringe of the Tibetan plateau, China. *Atmos. Environ.* 42: 970–979.
- Fu, X.W., Feng, X.B., Dong, Z.Q., Yin, R.S., Wang, J.X., Yang, Z.R. and Zhang, H. (2010a). Atmospheric gaseous elemental mercury (GEM) concentrations and mercury depositions at a high-altitude mountain peak in south China. *Atmos. Chem. Phys.* 10: 2425–2437.
- Fu, X.W., Feng, X.B., Zhang, G., Xu, W.H., Li, X.D., Yao, H., Liang, P., Li, J., Sommar, J., Yin, R.S. and Liu, N. (2010b). Mercury in the marine boundary layer and seawater of the South China Sea: Concentrations, sea/air flux, and implication for land outflow. *J. Geophys. Res.* 115: 6303.
- Fu, X.W., Feng, X.B., Qiu, G.L., Shang, L.H. and Zhang, H. (2011). Speciated atmospheric mercury and its potential source in Guiyang, China. *Atmos. Environ.* 45: 4205–4212.
- Fu, X.W., Feng, X.B., Shang, L.H., Wang, S.F. and Zhang, H. (2012a). Two years of measurements of atmospheric total gaseous mercury (TGM) at a remote site in Mt. Changbai area, Northeastern China. *Atmos. Chem. Phys.* 12: 4215–4226.

- Fu, X.W., Feng, X.B., Liang, P., Deliger, Zhang, H., Ji, J. and Liu, P. (2012b). Temporal trend and sources of speciated atmospheric mercury at Waliguan GAW station, Northwestern China. *Atmos. Chem. Phys.* 12: 1951–1964.
- Gustin, M.S., Huang, J.Y., Miller, M.B., Peterson, C., Jaffe, D.A., Ambrose, J., Finley, B.D., Lyman, S.N., Call, K., Talbot, R., Feddersen, D., Mao, H.T. and Lindberg, S.E. (2013). Do we understand what the mercury speciation instruments are actually measuring? Results of RAMIX. *Environ. Sci. Technol.* 47: 7295–7306.
- Hu, Q.H., Kang, H., Li, Z., Wang, Y.S., Ye, P.P., Zhang, L.L., Yu, J., Yu, X.W., Sun, C. and Xie, Z.Q. (2014). Characterization of atmospheric mercury at a suburban site of central China from wintertime to springtime. *Atmos. Pollut. Res.* 5: 769–778.
- Huang, J. and Gustin, M.S. (2015). Uncertainties of gaseous oxidized mercury measurements using KCl-coated denuders, cation-exchange membranes, and nylon membranes: Humidity influences. *Environ. Sci. Technol.* 49: 6102–6108.
- Jaffe, D., Prestbo, E., Swartzendruber, P., Weiss-Penzias, P., Kato, S., Takami, A., Hatakeyama, S. and Kajii, Y. (2005). Export of atmospheric mercury from Asia. *Atmos. Environ.* 39: 3029–3038.
- Landis, M.S., Stevens, R.K., Schaedlich, F. and Prestbo, E.M. (2002). Development and characterization of an annular denuder methodology for the measurement of divalent inorganic reactive gaseous mercury in ambient air. *Environ. Sci. Technol.* 36: 3000–3009.
- Li, Z., Xia, C.H., Wang, X.M., Xia, Y.R. and Xie, Z.Q. (2011). Total gaseous mercury in Pearl River Delta region, China during 2008 winter period. *Atmos. Environ.* 45: 834–838.
- Lin, C.J., Pongprueksa, P., Lindberg, S.E., Pehkonen, S.O., Byun, D. and Jang, C. (2006). Scientific uncertainties in atmospheric mercury models I: Model science evaluation. *Atmos. Environ.* 40: 2911–2928.
- Lindberg, S.E., Bullock, R., Ebinghaus, R., Engstrom, D., Feng, X.B., Fitzgerald, W., Pirrone, N., Prestbo, E. and Seigneur, C. (2007). A synthesis of progress and uncertainties in attributing the sources of mercury in deposition. *Ambio* 36: 19–32.
- Lyman, S.N., Gustin, M.S. and Prestbo, E.M. (2010). A passive sampler for ambient gaseous oxidized mercury concentrations. *Atmos. Environ.* 44: 246–252.
- McClure, C.D., Jaffe, D.A. and Edgerton, E.S. (2014). Evaluation of the KCl denuder method for gaseous oxidized mercury using HgBr₂ at an in-service AMNet site. *Environ. Sci. Technol.* 48: 11437–11444.
- Nair, U.S., Wu, Y., Walters, J., Jansen, J. and Edgerton, E.S. (2012). Diurnal and seasonal variation of mercury species at coastal-suburban, urban, and rural sites in the southeastern United States. *Atmos. Environ.* 47: 499–508.
- Nguyen, D.L., Kim, J.Y., Shim, S.G. and Zhang, X.S. (2011). Ground and shipboard measurements of atmospheric gaseous elemental mercury over the Yellow Sea region during 2007–2008. *Atmos. Environ.* 45: 253–260.
- Nguyen, H.T., Kim, M.Y. and Kim, K.H. (2010). The influence of long-range transport on atmospheric mercury on Jeju Island, Korea. *Sci. Total Environ.* 408: 1295–1307.
- Rutter, A.P. and Schauer, J.J. (2007). The effect of temperature on the gas – particle partitioning of reactive mercury in atmospheric aerosols. *Atmos. Environ.* 41: 8647–8657.
- Schroeder, W.H. and Munthe, J. (1998). Atmospheric mercury - An overview. *Atmos. Environ.* 32: 809–822.
- Slemr, F., Brunke, E.G., Ebinghaus, R. and Kuss, J. (2011). Worldwide trend of atmospheric mercury since 1995. *Atmos. Chem. Phys.* 11: 4779–4787.
- Subir, M., Ariya, P.A. and Dastoor, A.P. (2011). A review of uncertainties in atmospheric modeling of mercury chemistry I. Uncertainties in existing kinetic parameters - Fundamental limitations and the importance of heterogeneous chemistry. *Atmos. Environ.* 45: 5664–5676.
- van Loon, L., Mader, E. and Scott, S.L. (2000). Reduction of the aqueous mercuric ion by sulfite: UV spectrum of HgSO₃ and its intramolecular redox reaction. *J. Phys. Chem. A* 104: 1621–1626.
- Wang, Y.X., McElroy, M.B., Munger, J.W., Hao, J.M., Ma, H., Nielsen, C.P. and Chen, Y. (2008). Variations of O₃ and CO in summertime at a rural site near Beijing. *Atmos. Chem. Phys.* 8: 6355–6363.
- Wang, Z.W., Chen, Z.S., Duan, N. and Zhang, X.S. (2007). Gaseous elemental mercury concentration in atmosphere at urban and remote sites in China. *J. Environ. Sci. China* 19: 176–180.
- Xu, L.L., Chen, J.S., Yang, L.M., Niu, Z.C., Tong, L., Yin, L.Q. and Chen, Y.T. (2015). Characteristics and sources of atmospheric mercury speciation in a coastal city, Xiamen, China. *Chemosphere* 119: 530–539.
- Yang, Y.K., Chen, H. and Wang, D.Y. (2009). Spatial and temporal distribution of gaseous elemental mercury in Chongqing, China. *Environ. Monit. Assess.* 156: 479–489.
- Ye, Z., Mao, H., Lin, C.J. and Kim, S.Y. (2016). Investigation of processes controlling summertime gaseous elemental mercury oxidation at midlatitudinal marine, coastal, and inland sites. *Atmos. Chem. Phys.* 16: 8461–8478.
- Zhang, H., Fu, X.W., Lin, C.J., Wang, X. and Feng, X.B. (2015). Observation and analysis of speciated atmospheric mercury in Shangri-La, Tibetan Plateau, China. *Atmos. Chem. Phys.* 15: 653–665.
- Zhang, L., Wang, S.X., Wang, L. and Hao, J.M. (2013). Atmospheric mercury concentration and chemical speciation at a rural site in Beijing, China: Implication of mercury emission sources. *Atmos. Chem. Phys.* 13: 10505–10516.
- Zhu, J., Wang, T., Talbot, R., Mao, H., Hall, C.B., Yang, X., Fu, C., Zhuang, B., Li, S., Han, Y. and Huang, X. (2012). Characteristics of atmospheric Total Gaseous Mercury (TGM) observed in urban Nanjing, China. *Atmos. Chem. Phys.* 12: 12103–12118.

Received for review, September 18, 2016

Revised, November 21, 2016

Accepted, November 21, 2016